# CFD SIMULATION OF A CONICAL-CYLINDRICAL CRYSTALLIZATION UNIT USING MULTI-PHASE EULERIAN MODEL

**Khaled A. MAHDI[1]\*, Mohsen H. AL-RASHED[2], Ammar A. ALSAIRAFI[3] and Janusz WÓJCIK[4]**

[1]Chemical Engineering Department, Kuwait University, KUWAIT

[2]Department of Chemical Engineering, College of Technological Studies, PAAET, KUWAIT

[3]Mechanical Engineering Department, Kuwait University, KUWAIT

[4]Department of Chemical and Process Engineering, Silesian University of Technology, POLAND

*Corresponding author, E-mail address: khaled.mahdi@ku.edu.kw

## ABSTRACT

The effects of the shape of a crystallization unit bottom, diameter of the stirrer, its location and presence of the draft tube on: (i) unit power input distribution, (ii) average mixing power, (iii) pumping capacity are examined by mean of CFD simulations. Results indicate an optimal draft tube position between 0.35 and 0.5 $h_r/d_r$ and an optimal draft tube opening angle in the range of $8^o$ and $13^o$, in which hydraulic efficiency has the highest value. No elimination of circulation loops is observed within the aforementioned optimal configuration.

## NOMENCLATURE

$d_m$    diameter of impeller (m)
$D$    tank diameter (m)
$H_l$    draw tube's height (m)
$h_r$    the distance of draw tube (m)
$k$    turbulent kinetic energy ($m^2 \cdot s^{-2}$)
$K_p$    the number of pumping efficiency
$M_s$    torque momentum (N·m)
$n$    rotator speed (rps)
$Ne$    Newton's number (the power number)
$P$    power on the shaft of impeller (W)
$Re$    Reynolds's number
$u_z$    axial velocity ($m \cdot s^{-1}$)
$V_p$    volumetric flow of liquid through impeller ($m^3 \cdot s^{-1}$)
$\rho$    density of liquid ($kg \cdot m^{-3}$)
$\varepsilon$-    mean turbulent energy dissipation rate ($m^2 \cdot s^{-3}$)

## INTRODUCTION

Crystallization processes are usually carried out in agitated mixing tanks (Wachi and Jones, 1995). Conditions of mixing in crystallizers with internal circulation forced by mechanical stirrer significantly influence the final size of product crystals (Mersmann, 1999) and their characteristics. High levels of super-saturation around crystallization points in the mixer due to a cooling surface, evaporative interference and/or liquid reactants contact lead to an inhomogeneous solution and non-uniform mixing especially in fast precipitation systems. This causes very strong effects of homogeneous nucleation and possibly inhibits the growth of crystalline nuclei.

Imperfect mixing conditions are generally observed in most industrial crystallizers. They are caused by super-saturation phenomena, which create crystals of small final sizes, making downstream operations such as filtration difficult and inefficient (Mersmann, 1994). Moreover, the content of solution in the cake after filtration is too high, which lowers the quality of crystals considerably. This necessity complicates the filtration technology, raises costs of production and does not guarantee the expected specification of produced crystals.

Inhomogeneous solution and imperfect mixing conditions during processing justify the need for design optimization of the hydrodynamic conditions within the crystallizer. These conditions should be optimized to guarantee intensive macromixing (bulk) within the whole volume of the unit and simultaneously restrict the areas of strong micromimixing (local). They suppress formation of local high supersaturation zones, limit homogeneous nucleation phenomena so that any introduced substrates will undergo fast mixing with the whole content of the vessel (Cherzber, 1999). This is particularly important for sparingly soluble substances, which crystallize at large relative supersaturation of solution.

Proper selection of the internal geometrical configuration of the crystallizer will facilitate the following (a) right proportions of the reagents, (b) suitable type of stirrer, (c) required revolution frequency of the stirrer and (d) inlet place of individual reagents and outlet of product (Penicot, 1998). In spite of many theoretical and experimental works (Baldyga & Bourne 1999), there is still a lack of clear design principles permitting, without carrying out expensive experimental tests, to determine geometrical configuration and operating conditions of a crystallizer correctly. Computational Fluid Dynamics (CFD) with kinetic models of particulates processes can accommodate the multidimensionality of crystallization process, meaning all length scales from crystal size to crystallizer dimensions.

Computation Fluid Dynamics, CFD is the numerical analysis and solution of system involving transport processes via computer simulation (Jones et al., 2005). It involves the numerical solution of conservation equations continuity, momentum and energy equations coupled with constitutive laws of rate (kinetic) processes. Because crystallization involves a solid phase, a further

1

equation is required to account for the solid particles formed and destroyed during crystallization. This equation, known as
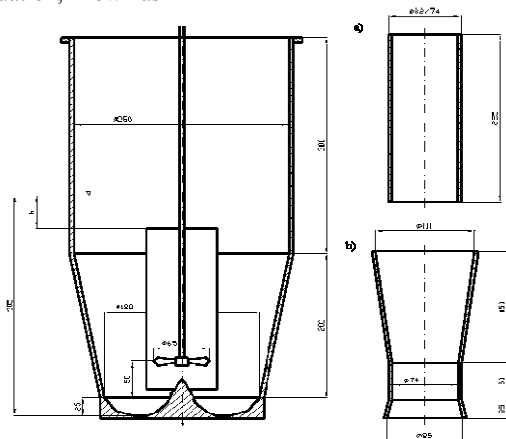


**Figure 1:** Conical-Cylindrical mixing unit.

the population balance, need to be solved simultaneously with transport rate equations for particle formation and destruction, in other words, a kinetic equation for crystallization. Consequently, the CFD model solution will comprise of flow properties as well as a particle size distribution. Besides modelling, there is the challenging task of creating a successful and a descriptive grid (mesh) that captures the geometry and configuration of the crystallizer (Al-Rashed and Jones, 1999). There are different types of grids, structured and unstructured grids and several grid generation techniques.

The investigators present their preliminary results of the CFD simulations, focused on the effect of geometrical configuration of a crystallizer onto energy dissipation rate, axial velocity field and mixing efficiency. Influence of the shape of unit bottom, diameter of the stirrer, its location and presence of the draft tube on: (i) unit power input distribution, (ii) average mixing power, (iii) pumping capacity were taken into consideration, respectively.

Obtained outcomes prove the existence of strong relationships between geometrical configuration of a crystallizer and the power input dissipation rate as well as mixing efficiency. In most cases, the CFD calculations are consistent with the experimental results and accessible literature data. However, further investigations are hindered due to the unavailability of advanced CFD programming modules and mesh generation techniques and expertise to incorporate hybrid CFD simulations of different crystallizer operating conditions and configurations. The later is the main motivation for this research proposal.

## SCOPE OF STUDY

This apparatus is widely used for continuous crystallization from the solution by means of adiabatic cooling method (vacuum method). The calculations were performed for homogeneous liquids in the range of turbulent flow and changing configuration of the internal equipment of the apparatus in the extent presented in Table 1.

| Circulation pipe (diameter x height (m)) | hr/dr | dm/D(D1) | Re |
|---|---|---|---|
| conical-cylindrical (0.074 x 0.225) | 0.2-0.49 | 0.36 | $1.38 \cdot 10^3$- $129 \cdot 10^3$ |

**Table 1:** Dimensions of the crystalizer.

The flow of suspension through the conical-cylindrical apparatus shown in Figure 1 was simulated using multiphase Eulerian model with standard k-ε method. The saturated solution of Ammonium Sulphate $(NH_4)_2SO_4$ and Potassium-Aluminium Sulphate $KAlSO_4.12H_2O$ were used as a model suspension. Table 2 shows the physical properties of these compounds.

| | $(NH_4)_2SO_4$ | $KAlSO_4.12H_2O$ |
|---|---|---|
| Solution density (kg/m$^3$) | 1244 | 1050 |
| Crystal density (kg/m$^3$) | 1769 | 1750 |
| Viscosity (Pa·s)·10$^3$ | 2,05 | 1,26 |
| Density difference (kg/m$^3$) | 525 | 700 |

**Table 2:** Physical Properties of model compounds.

For monodisperse suspension flow the mean particle size was assumed to be 0.35mm or 0.5mm and solid concentration as 10 vol.%. For polydisperse suspension flow 6 grain classes were assumed and solid concentration as 10 vol.% as shown in Table 3.

| Diameter (m)·10$^3$ | Concentration (m$^3$ solid/m$^3$ suspension) |
|---|---|
| 0.161695 | 0.1365 |
| 0.225 | 0.1329 |
| 0.2855 | 0.1924 |
| 0.3575 | 0.2402 |
| 0.45 | 0.1572 |
| 0.632898 | 0.1408 |

**Table 3:** Particle size distribution of polydisperse suspension.

## MODEL

For Eulerian multiphase calculations, FLUENT uses the phase coupled SIMPLE (PC-SIMPLE) algorithm (Vasquez and V. A. Ivanov , 2000) for the pressure-velocity coupling. PC-SIMPLE is an extension of the SIMPLE algorithm (Patankar, 1988) to multiphase flows. The velocities are solved coupled by phases, but in a segregated fashion. The block algebraic multigrid scheme used by the density-based solver described in (Weiss et al, 1999) is used to solve a vector equation formed by the velocity components of all phases simultaneously. Then, a pressure correction equation is built based on total volume continuity rather than mass

continuity. Pressure and velocities are then corrected so as to satisfy the continuity constraint.

### The Pressure-Correction Equation

For incompressible multiphase flow, the pressure-correction equation takes the form

$$\sum_{k=1}^{n}\frac{1}{\rho_{rk}}\left\{\frac{\partial}{\partial t}\alpha_k\rho_k\nabla\cdot\alpha_k\rho_k\vec{\upsilon}_k'+\nabla\cdot\alpha_k\rho_k\vec{\upsilon}_k^*\right\}=0 \qquad (1)$$

where $\rho_{rk}$ is the phase reference density for the $k^{th}$ phase (defined as the total volume average density of phase $k$), $\vec{\upsilon}_k'$ is the velocity correction for the $k^{th}$ phase, and $\vec{\upsilon}_k^*$ is the value of $\vec{\upsilon}_k$ at the current iteration. The velocity corrections are themselves expressed as functions of the pressure corrections.

### Volume Fractions

The volume fractions are obtained from the phase continuity equations. In discretized form, the equation of the $k^{th}$ volume fraction is

$$a_{p,k}\alpha_k = \sum_{nb}\left(a_{nb,k}\alpha_{nb,k}\right)+b_k = R_k \qquad (2)$$

$a_{a,k}$ is the relative velocity, $b_k$ represents the drift or the relative velocity. In order to satisfy the condition that all the volume fractions sum to one,

$$\sum_{k=1}^{n}\alpha_k = 1 \qquad (3)$$

### Fluid-Solid Exchange Coefficient

The fluid-solid exchange coefficient $K_{sl}$ can be written in the following general form:

$$K_{sl} = \frac{\alpha_s\rho_s f}{\tau_s} \qquad (4)$$

where $f$ is defined differently for the different exchange-coefficient models (as described below), and $\tau_s$, the "particulate relaxation time", is defined as

$$\tau_s = \frac{\rho_s d_s^2}{18\mu_l} \qquad (5)$$

where $d_s$ is the diameter of particles of phase $s$. All definitions of $f$ include a drag function ($C_D$) that is based on the relative Reynolds number ($Re_s$). It is this drag function that differs among the exchange-coefficient models.

For the model of (Wen and Yu, 1966) the fluid-solid exchange coefficient is of the following form:

$$K_{sl} = \frac{3}{4}C_D\frac{\alpha_s\alpha_l\rho_l\left|\vec{\upsilon}_s-\vec{\upsilon}_l\right|}{d_s}\alpha_l^{-2.65} \qquad (6)$$

where

$$C_D = \frac{24}{\alpha_l \, Re_s}\left[1+0.15\left(\alpha_l \, Re_s\right)^{0.687}\right] \qquad (7)$$

and $Re_s$ is defined by Equation (24)

$$Re_s = \frac{\rho_l d_s\left|\vec{\upsilon}_s-\vec{\upsilon}_l\right|}{\mu_l} \qquad (8)$$

where the subscript $l$ is for the $l^{th}$ fluid phase, $s$ is for the $s^{th}$ solid phase, and $d_s$ is the diameter of the $s^{th}$ solid phase particles.

## RESULTS

### Influence of the distance of draft tube from the bottom of the tank

The first parameter that was considered while simulating the process was the influence of the draft tube distance on pumping efficiency. Figure 2 shows the dependence of hydraulic efficiency of the apparatus (ratio of pumping efficiency number **Kp** to power number **Ne**) on the ratio $h_r/d_r$ (distance between draft tube and the bottom of the apparatus to the diameter of the tube). The influence of the distance of draft tube from bottom of the tank on the apparatus' hydraulic efficiency is evaluated for different flows: homogeneous saturated solution of ammonium sulphate ($\rho$=1244 (kg/m$^3$)), monodisperse suspension of ammonium sulphate of particle size of 0.35mm ($\rho$=1296.5 (kg/m$^3$)) as well as monodisperse suspension of alum of the particle size of 0.35mm ($\rho$=1120 (kg/m$^3$)). In all cases one can observe that the optimal draft tube position occurs between 0.35 and 0.55 $h_r/d_r$. Within this range the hydraulic efficiency achieves the highest values.

The decrease in hydraulic efficiency is noticeable for the alum suspension flow as compared to homogeneous solution. The suspension causes an increase in flow resistance due to flow inertia. It becomes imminent at the lower part of the mixer, where the suspension concentration is higher, the real field flow diminishes.
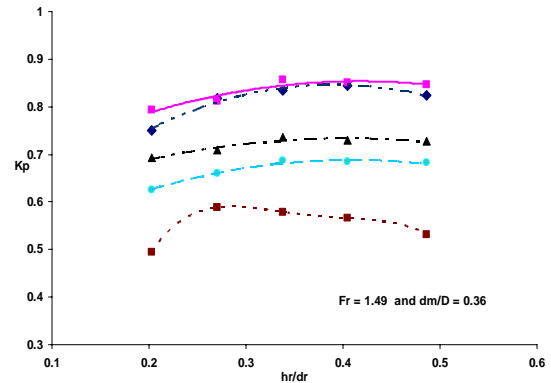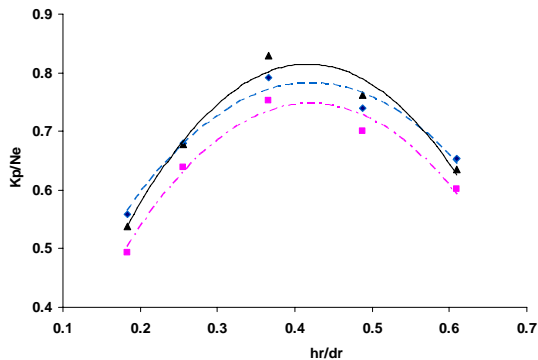


**Figure 2:** The Influence of the draft tube distance on pumping efficiency for: (♦) homogeneous solution (■) monodisperse suspension l=0.35mm, Δρ=525(kg/ m$^3$) (▲) monodisperse suspension l=0.35mm, Δρ=700(kg/m$^3$)

Comparing alum suspension flow to homogeneous solution of ammonium sulphate flow in the middle section, we observe an increase in the hydraulic efficiency of the apparatus. The alum suspension, having a lower density than ammonium sulphate solution, shows better hydraulic efficiency in this range. However, on the 'edges' of the system the hydraulic efficiency of the suspension is lower than for homogeneous liquid. The cause is attributed to a decrease in the velocity of flowing suspension that leads to an increase in solid concentration in lower part of apparatus resulting in a decrease in real flow section and additional flow resistance.
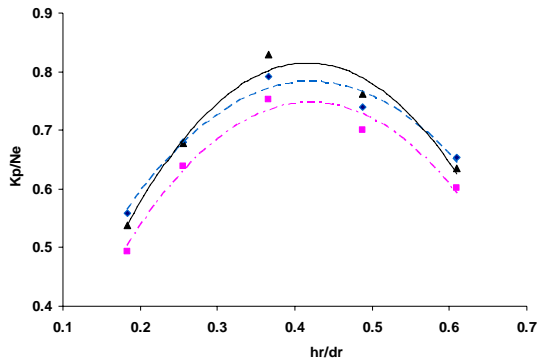
Figure 3 shows the influence of the draft tube distance on hydraulic efficiency of the apparatus for the flow of monodisperse suspensions of ammonium sulphate and alum for two particle sizes: 0.35mm and 0.5mm. It can be noticed that the area of the best hydraulic efficiency is for the draft tube distance within the range of 0.35 and 0.5 $h_r/d_r$. Higher hydraulic efficiency for alum is caused by the lower suspension density. The power number is inversely proportional to the density.



**Figure 3:** The Influence of the draft tube distance on the hydraulic efficiency of the apparatus for: (×) monodisperse alum suspension l=0.5mm, $\Delta\rho$=700(kg/m$^3$), (▲) monodisperse alum suspension l=0.35mm, $\Delta\rho$=700(kg/m$^3$) (■) monodisperse ammonia sulfate suspension

When the distance between the draft tube and the bottom of the apparatus is large, a significant decrease in the hydraulic efficiency is observed, especially for alum. For maximal distance in the investigated area i.e. 0.6 $h_r/d_r$, and for the particles of the diameter of 0.5mm and density difference of $\Delta\rho$=700(kg/m$^3$), the condition of 'just suspended' is not preserved. The solid settles at the bottom and does not circulate. That is why there is no measurement point for alum of the particle size of 0.5mm.

The optimal draft tube distance with respect to hydraulic efficiency is always within the range of 0.35 and 0.5 $h_r/d_r$, regardless of the suspension polydispersity, as illustrated in
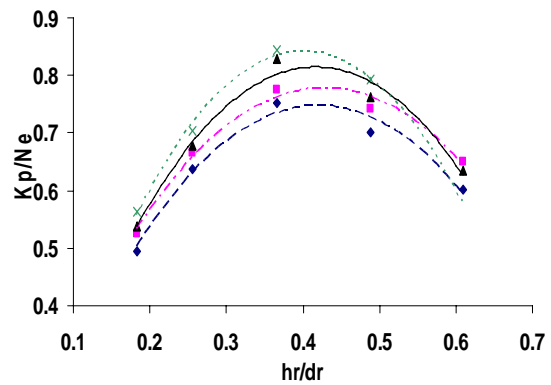


 Figure 4. However, the hydraulic efficiency of the apparatus declines in the case of polydisperse suspension flow, in comparison to monodisperse suspension flow due to the lower porosity of the polydisperse bed in the gap between the draft tube and the bottom of the tank as a result of the increase in flow resistance.

Regardless of polydispersity, the flow of alum suspension has higher hydraulic efficiency in comparison with the ammonium sulphate suspension. However, when the distance between the draft tube and apparatus bottom is large, the decrease of velocity in the gap between the draft tube and the bottom appears. This leads to the increase in solid concentration at the bottom, particularly large particles. Such accumulation is noticeable more for alum due to the larger density differences that results in the increase of flow resistance.

The ammonium sulphate bed porosity distribution is shown for both monodisperse (Figure 5a) and polydisperse (Figure 5b) suspension. The distribution suggests that solid distribution is similar in both cases regardless of the polydispersity. Accumulation of solid on the internal walls of draft tube as well as at the bottom of the apparatus takes place. In the region of mixing shaft and in the vicinity of the external walls of the draft tube, solid almost does not appear to be present. Such suspension distribution is attributed to the centrifugal forces.

4
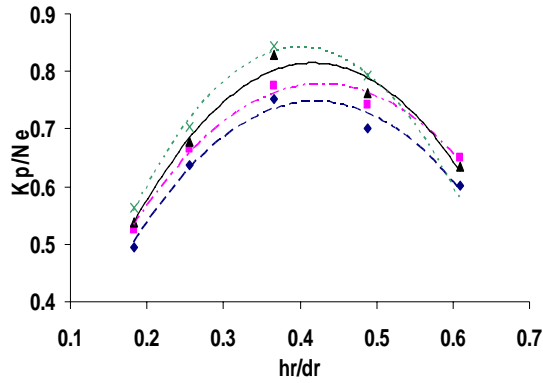
**Figure 4:** The Influence of the draft tube distance on hydraulic efficiency of the apparatus for: (■) monodisperse suspension l=0.35mm, $\Delta\rho$=700(kg/m³), (♦) monodisperse suspension l=0.35mm, $\Delta\rho$=500(kg/m³), (×) polydisperse suspension, $\Delta\rho$=700(kg/m³), (▲) polydisperse =500(kg/m³).

The ammonium sulphate bed porosity distribution is shown for both monodisperse (Figure 5a) and polydisperse (Figure 5b) suspension. The distribution suggests that solid distribution is similar in both cases regardless of the polydispersity. Accumulation of solid on the internal walls of draft tube as well as at the bottom of the apparatus takes place. In the region of mixing shaft and in the vicinity of the external walls of the draft tube, solid almost does not appear to be present. Such suspension distribution is attributed to the centrifugal forces.

Lower porosity of the polydisperse suspension bed at the bottom of the apparatus (blue colour in Figure 5b) leads to flow field reduction hence increase in flow resistance.
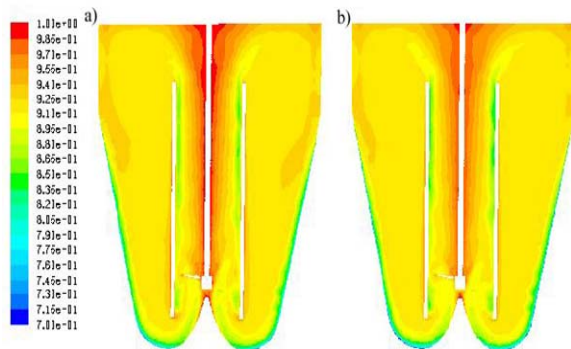


**Figure 5:** Bed porosity distribution in DTM apparatus of the draft tube distance of hr/dr=0.36, **$\Delta\rho$** =500(kg/m³) monodisperse suspension l=0.35mm, b) polydisperse suspension

### Influence of the draft tube opening angle

Basing on the research conducted for homogeneous fluid flow one suggests that application of the conical draft tube causes increase in pumping efficiency of agitator and reduces power consumption. An optimal opening angle of the draft tube at the maximal hydraulic efficiency of the apparatus is evaluated. Four different draft tube angles are used in calculations: 0°, 6.5°, 13° and 19.4°; shown in **Figure 6**.
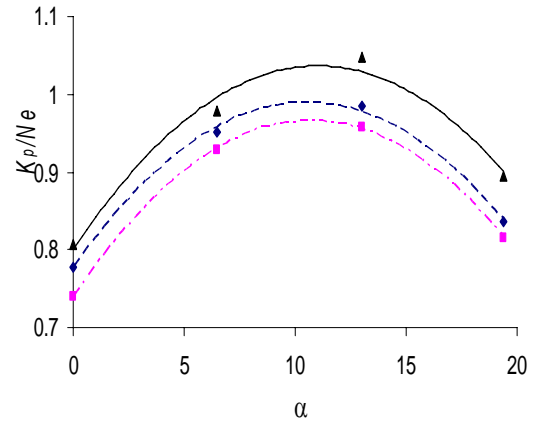


**Figure 6:** The Influence of the draft tube opening angle on the hydraulic efficiency of the apparatus for: (×) monodisperse alum suspension l=0.5mm, $\Delta\rho$=700(kg/m³), (▲) monodisperse alum suspension l=0.35mm, $\Delta\rho$=700(kg/m³) (■) monodisperse ammonia sulphate suspension $\Delta\rho$=500(kg/m³).

For different angles, the effect of the draft tube opening angle on the hydraulic efficiency of the apparatus is compared for different flows: monodisperse suspension of alum of the particle size 0.5mm ($\rho$=1120 (kg/m³)), polydisperse suspension of alum ($\rho$=1120 (kg/m³)) and polydisperse suspension of ammonium sulphate ($\rho$=1296,5 (kg/m³)). In all cases, an optimal value of the draft tube opening angle exists between 8° and 13°. In this range, the hydraulic efficiency is maximum.

The flow profiles for homogeneous fluid and polydysperse suspension are presented in Figure 7. Presence of solid in the investigated cases did not have influence on flow profile in the apparatus. In all examined configurations, circulation loops are present at the outlet of the draft tube. Formation of those loops causes energy dissipation.

### CONCLUSION

The application of the appropriate configuration of the crystallizer causes significant improvement in the hydraulic efficiency of the apparatus. There exist an optimal draft tube position between 0.35 and 0.5 $h_r/d_r$ and an optimal draft tube opening angle in the range of 8° and 13° at which the hydraulic efficiency is maximum. However, such conditions are not sufficient to eliminate circulation loops which presence creates additional energy dissipation affecting the crystallization. Intensive agitation, to overcome the energy dissipation, at the surface of the crystallizer allow to unload the supersaturation.

### ACKNOWLEDGEMENT
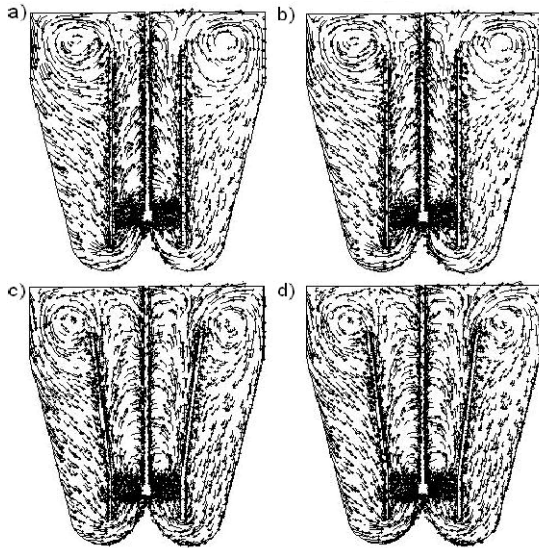
**Figure 7**: Fluid flow profiles: a,c –mother liquid, b,d – polydisperse suspension

## REFERENCES

BIGDA, J., (2005), "Determination of specific working parameters of mixers CFD", *the silesian university of technology*,

PLEWIK, R., (2005), "Determination of the power number and the pumping efficiency for draft tube tank", MSc, *The Silesian University of technology Gliwice*,

IBRAHIM, S. and NIENOW, A. W., (1995), "Power curves", *Trans. IChemE (Part A)*, **73**, 485-491.

CHUDACEK, M. W., (1985), "Impeller Power numbers and impeller flow numbers in profiled bottom tanks", *Ind.Eng.chem.process des. dev*, **24**,

JONES, A. G. and MULLIN, J. W., (1973), "the design of draft-tube agitated vessel", *chemistry and industry*

MARSHALLA, E. M. and BAKKER, A., (2003), "computational fluid mixing ",

PLEWIK, R., (2005), "Determination of the power number and the pumping efficiency for draft tube tank ", MSc, *the silesian university of technology*

VASQUEZ, S. A. and IVANOV, V. A., (2000), "A Phase Coupled Method for Solving Multiphase Problems on Unstructured Meshes", *ASME FEDSM'00: ASME 2000 Fluids Engineering Division Summer Meeting*,

JONNES, A., RIGOPOLOUS, S. and ZAUNER, R., (2005), "Crystallization and precipitation Engineering", *Chem. Eng. Comp.* , **29**, 1159-1166.

MERSMANN, A., (1999), "Crystallization and precipitation", *Chem. Eng. Process.*, **39**, 345-353.

MERSMANN, A., ANGERHOFER, M. and FRANK, J., (1994), "Controlled Precipitation", *Chem. Eng. Techn.*, **17**, 1-9.

CHERZBERG, H., KAHLE, K. and KASEBERG, K., (1999), "Continuous Precipitation and Reaction Crystallization of Inorganic Substances in Agitated Crystallizers with an Integrated Clarification Zone", *Chem. Eng. Techn.*, **21**, 412-417.

PENICOT, P. and OTHERS, (1998), "Influence of the Internal Crystallizer Geometry and the Operational Conditions on the solid Product Quality", *Chem. Eng. Techn.*, **21**, 507-514.

BAŁDYGA, J. and BOURNE, (1999), "Turbulent Mixing and Chemical Reactions", John Wiley and Sons,

PATANKAR, S. V., (1980), " Numerical Heat Transfer and Fluid Flow", Hemisphere

WEISS, J. M., MARUSZEWSKI, J. P. and SMITH, W. A., (1999), "Implicit Solution of Preconditioned Navier-Stokes Equations Using Algebraic Multigrid", *AIAA Journal*, **37**, 29-36.

WEN, C. Y. and YU, Y. H., (1966), "Mechanics of Fluidization", *Chem. Eng. Prog. Symp. Series*, **62**, 100-111.

RICHARDSON, J. R. and ZAKI, W. N., (1954), "Sedimentation and Fluidization: Part I", *Trans. Inst. Chem. Eng.*, **32**, 35-53.

WACHI, S. and JONES, A., (1995), "Aspects of gas-liquid reaction systems with precipitate particle formation", *Reviews in Chemical Engineering*, **11**, 1.

AL-RASHED, M. H. and JONES, A. G., (1999), "CFD modelling of gas-liquid reactive precipitation", *Chem. Eng. Sci.*, **54**, 4779-4784.

WEI, H. and GARSIDE, J., (1997), "Application of CFD modelling to precipitation systems", *Trans. IChemE Part A*, **75**, 219.

WÓJCIK, J. A. and JONES, A. G., (1998), "Particle disruption of precipitated CaCO3 crystal agglomerates in turbulently agitated suspensions", *Chem. Eng. Sci.*, **53**, 1097-1101.